

# Spectral analysis of Kepler SPB and $\beta$ Cep candidate stars<sup>★</sup>

H. Lehmann<sup>1</sup>, A. Tkachenko<sup>1</sup>, T. Semaan<sup>2</sup>, J. Gutiérrez-Soto<sup>2,3</sup>, B. Smalley<sup>4</sup>, M. Briquet<sup>5</sup>, D. Shulyak<sup>6</sup>, V. Tsymbal<sup>7</sup>,  
and P. de Cat<sup>8</sup>

<sup>1</sup> Thüringer Landessternwarte Tautenburg, 07778 Tautenburg, Germany  
e-mail: lehm@tls-tautenburg.de, andrew@tls-tautenburg.de

<sup>2</sup> GEPI, Observatoire de Paris, CNRS, Université Paris Diderot, 5 place Jules Janssen, 92190 Meudon, France  
e-mail: thierry.semaan@obspm.fr

<sup>3</sup> Instituto de Astrofísica de Andalucía (CSIC), Apartado 3004, 18080 Granada, Spain, e-mail: jgs@iaa.es

<sup>4</sup> Astrophysics Group, Keele University, Staffordshire, ST5 5BG, United Kingdom, e-mail: bs@astro.keele.ac.uk

<sup>5</sup> Instituut voor Sterrenkunde, Katholieke Universiteit Leuven, Belgium, e-mail: maryline@ster.kuleuven.be

<sup>6</sup> Georg-August-University, Göttingen, Germany, e-mail: denis.shulyak@gmail.com

<sup>7</sup> Taurian National University, Department of Astronomy, Simferopol, Ukraine, e-mail: vadim@starsp.org

<sup>8</sup> Royal Observatory of Belgium, e-mail: peter@oma.be

Received ; accepted

## ABSTRACT

**Context.** For an asteroseismic modeling, the analysis of the high-accuracy light curves delivered by the Kepler satellite mission needs support by ground-based multi-colour and spectroscopic observations.

**Aims.** We determine the fundamental parameters of SPB and  $\beta$  Cep candidate stars observed by the Kepler satellite mission and estimate the expected types of non-radial pulsators.

**Methods.** We compare newly obtained high-resolution spectra with synthetic spectra computed on a grid of stellar parameters assuming LTE and check for NLTE effects for the hottest stars. For comparison, we determine  $T_{\text{eff}}$  independently from fitting the spectral energy distribution of the stars obtained from the available photometry.

**Results.** We determine  $T_{\text{eff}}$ ,  $\log g$ , micro-turbulent velocity,  $v \sin i$ , metallicity, and elemental abundance for 14 of the 16 candidate stars, two of the stars are spectroscopic binaries. No significant influence of NLTE effects on the results could be found. For hot stars, we find systematic deviations of the determined effective temperatures from those given in the Kepler Input Catalogue. The deviations are confirmed by the results obtained from ground-based photometry. Five stars show reduced metallicity, two stars are He-strong, one is He-weak, and one is Si-strong. Two of the stars could be  $\beta$  Cep/SPB hybrid pulsators, four SPB pulsators, and five more stars are located close to the borders of the SPB instability region.

**Key words.** Asteroseismology – Stars: early-type – Stars: variables: general – Stars: atmospheres – Stars: abundances

## 1. Introduction

The Kepler satellite delivers light curves of unique accuracy and time coverage, providing unprecedented data for the asteroseismic analysis. The identification of non-radial pulsation modes and the asteroseismic modeling, on the other hand, require a classification of the observed stars in terms of  $T_{\text{eff}}$ ,  $\log g$ ,  $v \sin i$ , and metallicity. These basic stellar parameters can only be obtained from the colors of the stars which are not measured by the satellite. That is why ground-based multi-colour and spectroscopic observations of the Kepler target stars are urgently needed. We describe a semi-automatic method of spectrum analysis based on high-resolution spectra of stars in the Kepler satellite field of view that have been proposed by the Working Groups 3 and 6 of the Kepler Asteroseismic Science Consortium (KASC) to be candidates for SPB and  $\beta$  Cep pulsators.

The object selection was mainly based on the data given in Kepler Input Catalogue (KIC). The spectral types given for these stars in the SIMBAD database are based on only a few, older measurements and in most cases no luminosity class is given.

For the KIC data, on the other hand, an uncertainty of the surface gravity of  $\pm 0.5$  dex is stated in the catalogue, much too high for an accurate classification in terms of non-radial pulsators, and there are hints that the temperature values given in the KIC show larger deviations for the hotter stars (see Molenda-Żakowicz et al. 2010). For two of the selected stars we found no classification in the SIMBAD database and for two no classification in the KIC.

The aim of this work is to provide fundamental stellar parameters like effective temperature  $T_{\text{eff}}$ , surface gravity  $\log g$ , metallicity  $\epsilon$ , and projected rotation velocity  $v \sin i$  for an asteroseismic modeling of the stars, to compare our results of spectral analysis with the KIC data and to estimate the expected type of variability of the different target stars.

For the analysis, we used stellar atmosphere models and synthetic spectra computed under the LTE assumption. The advantage of the applied programs (see Sect. 3) is that they allow to use different metallicity and individual abundances of He and metals and that they are running fast in parallel mode on a cluster PC installed at TLS.

In the investigated spectral region, the spectra of the B-type stars are dominated by the He I lines. Auer & Mihalas (1973) state that we have to expect deviations in the equivalent widths of the He lines due to the effects of departure from local thermo-

<sup>★</sup> Based on observations with the 2-m Alfred Jensch telescope at the Thüringer Landessternwarte (TLS) Tautenburg.

**Table 1.** List of observed stars.

KIC	designation	type	$V$	$N$	$S/N$
3 240 411	GSC 03135–00115	$\beta$ Cep	10.2	2	67
3 756 031	GSC 03135–00619	$\beta$ Cep	10.0	2	80
5 130 305	HD 226 700	SPB	10.2	2	74
5 217 845	HD 226 628	SPB	9.3	2	103
5 479 821	HD 226 795	SPB	9.9	1	65
7 599 132	HD 180 757	SPB	9.3	1	75
8 177 087	HD 186 428	SPB, $\beta$ Cep	8.1	1	138
8 389 948	HD 189 159	SPB	9.1	1	81
8 451 410	HD 188 459	SPB	9.1	2	104
8 459 899	HD 190 254	$\beta$ Cep	8.7	2	127
8 583 770	HD 189 177	SPB	10.1	2	74
8 766 405	HD 187 035	SPB, $\beta$ Cep	8.8	1	103
10 960 750	BD+482 781	SPB, $\beta$ Cep	9.7	1	59
11 973 705	HD 234 999	SPB	9.1	2	116
12 207 099	BD+502 787	$\beta$ Cep	10.3	2	69
12 258 330	HD 234 893	SPB, $\beta$ Cep	9.3	2	105

dynamic equilibrium (LTE) for stars in the 15 000 to 27 500 K temperature range in the order of 10% for  $4026 \text{ \AA} < \lambda < 5047 \text{ \AA}$  and of up to 30% for the  $5 876 \text{ \AA}$  line. There is a controversial discussion about these results, however (see Sect. 6.1). For that reason, to check for the reliability of our results of the spectral analysis obtained in the LTE regime, we repeated the analysis for the four hottest stars of our sample using programs with non-local thermodynamic equilibrium (NLTE) capability (Sect. 4) but had to assume constant, solar metallicity and He abundance.

One further test is described in Sect. 5, where we derive the effective temperatures of the stars from their available photometry and try to explain the deviations of the  $T_{\text{eff}}$  given in the KIC from our spectroscopically determined values. The results obtained from the different methods are discussed in Sect. 6.

## 2. Observations and spectrum reduction

Spectra of 16 bright ( $V < 10.4$ ) suspected SPB and  $\beta$  Cep stars selected from the KIC have been taken with the Coude-Echelle spectrograph attached to the 2-m telescope at the Thüringer Landessternwarte (TLS) Tautenburg. The spectra have a resolution of 32 000 and cover the wavelength range from 470 to 740 nm. Table 1 gives KIC number, common designation, suspected type of variability,  $V$ -magnitude, number of observed spectra, and the signal-to-noise of the averaged spectra for all observed stars. Spectra have been reduced using standard ESO-MIDAS packages. The reduction included filtering of cosmic rays, bias and stray light subtraction, flat fielding, optimum extraction of the Echelle orders, wavelength calibration using a Th-Ar lamp, normalization to the local continuum, and merging of the orders. Small shifts of the instrumental zero-point have been corrected by an additional wavelength calibration using a large number of telluric  $\text{O}_2$ -lines. Finally, the difference in the radial velocities (RVs) between all spectra of the same star have been determined from cross-correlation and the spectra have been rebinned according to these differences and added to build the mean, averaged spectrum.

## 3. LTE based analysis

### 3.1. The method

Due to the large  $v \sin i$  of many of the observed stars it is impossible to find a sufficiently large number of unblended spectral lines for a spectral analysis based on the comparison of the

equivalent widths of the lines of single elements. Thus we decided to analyse the spectra by computing synthetic spectra for a wider spectral region, including  $\text{H}_\beta$  and a larger number of metal lines. We used the range from 472 to 588 nm (lower end of the covered wavelength range up to the wavelength where stronger telluric lines occur).

We used the LLmodels program (Shulyak et al. 2004) in its most recent parallel version to compute the atmosphere models and the SynthV program (Tsymbal 1996) in a parallelized version written by A.T. to compute the synthetic spectra. The LLmodels code is a 1-D stellar model atmosphere code for early and intermediate type stars assuming LTE which is intended for as accurate a treatment as possible of the line opacity using a direct method for the line blanketing calculation. This line-by-line method is free of any approximations so that it fully describes the dependence of the line absorption coefficient on frequencies and depths in a model atmosphere, it does not require pre-calculated opacity tables. The code is based on modified ATLAS9 subroutines (Kurucz 1993a) and the continuum opacity sources and partition functions of iron-peak elements from ATLAS12 (Kurucz 1993b) are used. Like the SynthV program, it can handle individual elemental abundances. Actually, the main limitation with respect to hot stars is that both programs assume LTE.

The line tables have been taken from the VALD data base (Kupka et al. 2000). They are adjusted by the mentioned programs according to the different spectral types. For the comparison with the synthetic spectra, the observed spectra have been rebinned in wavelength according to their RVs obtained from the cross-correlation with the computed spectra and averaged in the case of several observations per star.

We computed the synthetic spectra on a grid in  $T_{\text{eff}}$ ,  $\log g$ ,  $v \sin i$ , and metallicity  $\epsilon$ , based on a pre-calculated library of atmosphere models. The models have been computed by scaling the solar metal abundances according to the different metallicities from  $-0.8$  to  $+0.8$  dex, assuming constant, solar He abundance and a micro-turbulent velocity of  $2 \text{ km s}^{-1}$ . At this point, we derived the value of the metallicity and its error that we will give later in Table 5.

In a second step, we fixed the previously derived parameters to its optimum values and took the abundance table corresponding to the determined metallicity as the starting point to readjust the abundances of He and all metals for which we found measurable contributions in the observed spectra. Here, we iterated the individual abundances together with  $v \sin i$ .

In the final step, we readjusted the values of  $T_{\text{eff}}$ ,  $\log g$ , and  $v \sin i$  based on the abundances determined in step two and added the micro-turbulent velocity  $\xi_t$  as a free parameter. We were not able to compute all the atmosphere models for the full parameter space including the individual abundances of He and metal lines and different  $\xi_t$ , however. We used the atmosphere models computed for the fixed, optimum metallicity determined in step 1 but computed the synthetic spectra with the SynthV program based on the individual abundances determined in step 2. A comparison of the derived metallicities and metal abundances showed that the derived values are compatible in most cases. Only for the three stars where we found larger deviations of the He abundance (the He weak star KIC 5 479 821 and the He strong stars KIC 8 177 087 and KIC 12 258 330), we had to calculate and use atmosphere models based on exactly the determined He abundances. The final values of the parameters and its errors have been taken from step 1 for the metallicity, from step 2 for the individual abundances (here, we did no error calculation but assume the error derived for the metallicity to be the typical error), and from the last step for all the other parameters.

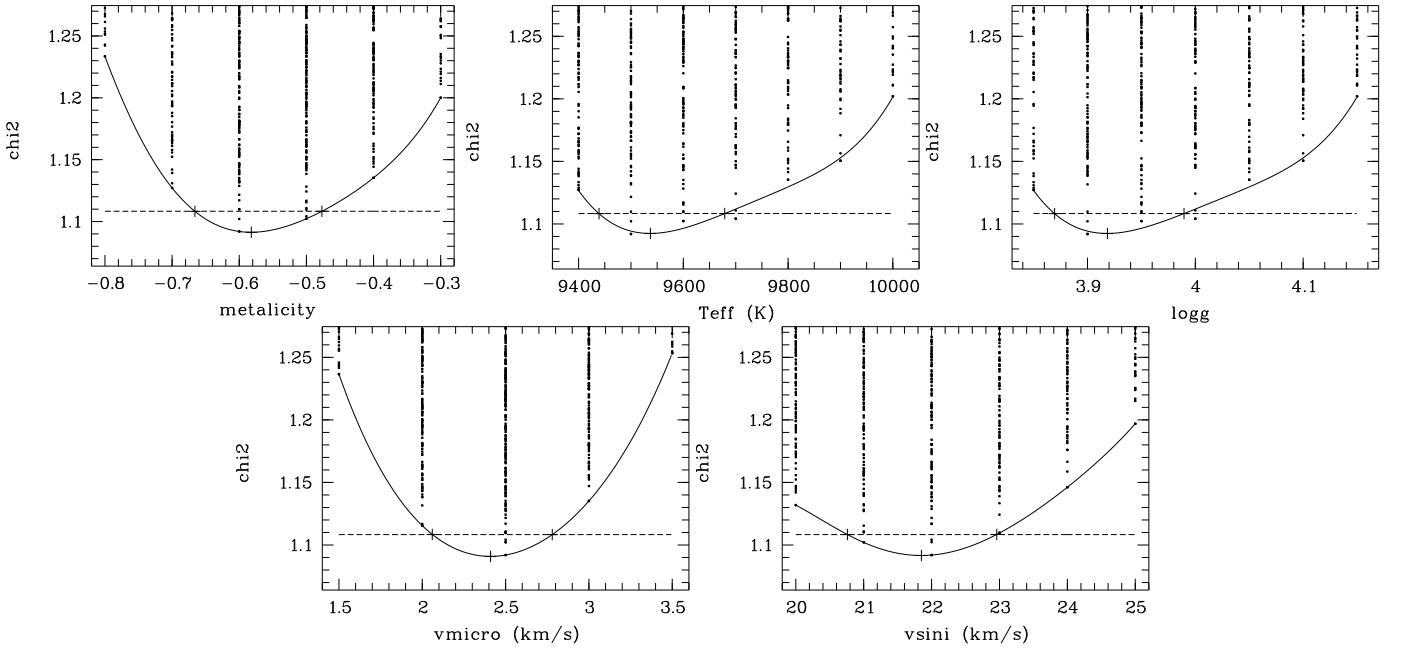


**Fig. 1.**  $\chi^2$  values obtained from the 5-dimensional grid versus the 5 different parameters.

The applied method of grid search allows to find the global minimum of  $\chi^2$  and for a realistic estimation of the errors of the parameters as we will show in the next section.

### 3.2. Testing the method

The method has been tested on a spectrum of Vega taken with the same instrument and resolution, with the aim to check for the reliability of the obtained values and for the influence of the different parameters on the accuracy of the results. Fig. 1 shows the  $\chi^2$ -distributions obtained from the grid search. Each panel contains all  $\chi^2$  values up to a certain value obtained from all combinations of the different parameters versus one of the parameters. The dashed lines indicate the  $1\sigma$  confidence level obtained from the  $\chi^2$ -statistics assuming that for a large number of degrees of freedom, the  $\chi^2$ -distribution approaches a Gaussian one. The continuous curves show the polynomial fit to the smallest  $\chi^2$ -values. The three crosses in each panel show the optimum value and the  $\pm 1\sigma$  error limits of the corresponding parameter.

Table 2 lists the resulting values. Table 3 compares the results with values from the literature. Our values of  $T_{\text{eff}}$  and  $\log g$  agree well with those from previous investigations. The metallicity and micro-turbulent velocity have been used by us as free parameters as well. The obtained values confirm those assumed by the other authors and the obtained value of  $v \sin i$  is identical with that measured by Hill et al. (2004).

Table 4 gives the fraction of the computed error of each parameter in the case of fixing one of the parameters to the error computed when all parameters are considered to be free. The values indicating the largest effects are set in bold face. It shows that there is a strong correlation between  $T_{\text{eff}}$ ,  $\log g$ , and metallicity. This can be easily understood because the line strengths are determined by  $T_{\text{eff}}$  and  $\epsilon$  and the shape of the Balmer line is strongly influenced by  $\log g$  and  $\epsilon$ .  $v \sin i$  and  $\xi_t$ , on the other hand, are much less influenced by the other parameters and fixing them to their optimum values in the error calculation has no effect on the derived errors of the other parameters. The result

**Table 2.** Fundamental parameters of Vega obtained from grid search.

$T_{\text{eff}} = 9540_{-100}^{+140}$ K	$\xi_t = 2.41_{-0.35}^{+0.37}$ km s $^{-1}$	$\log(g) = 3.92_{-0.05}^{+0.07}$
$v \sin(i) = 21.9_{-1.1}^{+1.1}$ km s $^{-1}$	$\epsilon = -0.58_{-0.08}^{+0.10}$ dex	

**Table 3.** Vega: Comparison of the results.

model	$T_{\text{eff}}$ K	$\log g$	$\epsilon$	$\xi_t$ km s $^{-1}$	$v \sin i$ km s $^{-1}$
1) ATLAS 6	9 400	3.95	0.0	2.0	
2) MARCS	9 650	3.90	0.0	3.0	
3) ATLAS 6	9 500	3.90	0.0	2.0	
4) ATLAS 6	9 500	3.90	-0.5	2.0	
5) ATLAS 12	9 550	3.95	-0.5	2.0	
6) ATLAS 9	9 506	4.00	-0.6	1.1	21.9
7) LLmodels	9 540	3.92	-0.58	2.4	21.9

1) Kurucz (1979), 2) Dreiling & Bell (1980), 3) Lane & Lester (1984), 4) Gigas (1986), 5) Castelli & Kurucz (1994), 6) Hill et al. (2004), 7) our result

**Table 4.** Reduction in the errors of the parameters in % by fixing one of them.

$\epsilon$	$\xi_t$	$\log(g)$	$T_{\text{eff}}$	$v \sin(i)$
fixed	86	<b>67</b>	<b>64</b>	98
100	fixed	100	100	100
<b>56</b>	81	fixed	<b>39</b>	77
<b>56</b>	78	<b>50</b>	fixed	95
100	97	100	98	fixed

shows that we have to vary at least  $T_{\text{eff}}$ ,  $\log g$ , and metallicity together to get reliable error estimations for each single parameter.

**Table 5.** Fundamental parameters.  $T_{\text{eff}}^{\text{K}}$  and  $\log g^{\text{K}}$  are taken from the KIC and given for comparison. Stars are sorted by their KIC number.

KIC	$T_{\text{eff}}^{\text{K}}$	$T_{\text{eff}}$	$\frac{1\sigma}{T_{\text{eff}}}$	$\log g^{\text{K}}$	$\log g$	$1\sigma$	$\xi_i$	$1\sigma$	$v \sin i$	$\frac{1\sigma}{v \sin i}$	spectral type		
	K	%	CDS							KIC	new		
3 240 411		20980 <sup>+880</sup> <sub>-840</sub>	4.1		4.01 <sup>+0.12</sup> <sub>-0.11</sub>	0.11	4.8 <sup>+2.9</sup> <sub>-4.7</sub>	3.8	42.6 <sup>+5.1</sup> <sub>-4.9</sub>	11	–	–	B2 V
3 756 031	11 177	15 980 <sup>+310</sup> <sub>-300</sub>	1.9	4.24	3.75 <sup>+0.06</sup> <sub>-0.06</sub>	0.06	0.5 <sup>+2.3</sup> <sub>-0.5</sub>	2.3	30.8 <sup>+3.8</sup> <sub>-3.1</sub>	11	–	B8.5 V	B5 V-IV
5 130 305	9 533	10 670 <sup>+180</sup> <sub>-200</sub>	1.8	4.14	3.86 <sup>+0.07</sup> <sub>-0.07</sub>	0.07	1.4 <sup>+0.7</sup> <sub>-1.0</sub>	0.8	155 <sup>+13</sup> <sub>-13</sub>	8.4	B9	A0 V	B9 V-IV
5 217 845 <sup>1)</sup>	8 813	11 790 <sup>+240</sup> <sub>-260</sub>	2.1	3.70	3.41 <sup>+0.10</sup> <sub>-0.08</sub>	0.09	2.1 <sup>+0.8</sup> <sub>-0.9</sub>	0.8	237 <sup>+16</sup> <sub>-16</sub>	6.8	B8	A3 IV	B8.5 III
5 479 821	10 850	14 810 <sup>+350</sup> <sub>-290</sub>	2.2	4.19	3.97 <sup>+0.09</sup> <sub>-0.07</sub>	0.08	0.1 <sup>+1.3</sup> <sub>-0.1</sub>	1.3	85 <sup>+8</sup> <sub>-8</sub>	9.4	B8	B9 V	B5.5 V
7 599 132	10 251	11 090 <sup>+100</sup> <sub>-140</sub>	1.1	3.62	4.08 <sup>+0.06</sup> <sub>-0.06</sub>	0.06	1.6 <sup>+0.5</sup> <sub>-0.6</sub>	0.6	63 <sup>+5</sup> <sub>-4</sub>	7.1	B9	B9.5 IV	B8.5 V
8 177 087	9 645	13 330 <sup>+220</sup> <sub>-170</sub>	1.5	4.10	3.42 <sup>+0.06</sup> <sub>-0.06</sub>	0.06	1.3 <sup>+0.5</sup> <sub>-0.7</sub>	0.6	22.2 <sup>+1.5</sup> <sub>-1.7</sub>	7.2	B9	A0 V	B7 III
8 389 948	8 712	10 240 <sup>+340</sup> <sub>-220</sub>	2.7	3.61	3.86 <sup>+0.12</sup> <sub>-0.10</sub>	0.11	0.8 <sup>+0.9</sup> <sub>-0.8</sub>	0.9	142 <sup>+12</sup> <sub>-11</sub>	8.1	B9 V	A3 IV	B9.5 V-IV
8 451 410 <sup>2)</sup>	8 186	8 490 <sup>+100</sup> <sub>-100</sub>	1.2	3.81	3.51 <sup>+0.07</sup> <sub>-0.05</sub>	0.06	3.8 <sup>+0.4</sup> <sub>-0.4</sub>	0.4	39.8 <sup>+1.4</sup> <sub>-1.4</sub>	3.5	B9 V	A5 IV	A3.5 IV-III
8 459 899 <sup>3)</sup>	9 231	15 760 <sup>+240</sup> <sub>-210</sub>	1.4	4.22	3.81 <sup>+0.05</sup> <sub>-0.05</sub>	0.05	1.4 <sup>+1.6</sup> <sub>-1.4</sub>	1.5	53 <sup>+4</sup> <sub>-4</sub>	7.5	B8	A1 V	B4.5 IV
8 583 770	7 659	9 690 <sup>+230</sup> <sub>-170</sub>	2.1	3.47	3.39 <sup>+0.08</sup> <sub>-0.05</sub>	0.07	1.3 <sup>+0.6</sup> <sub>-0.8</sub>	0.7	102 <sup>+9</sup> <sub>-7</sub>	7.8	B9	A7 IV-III	A0.5 IV-III
8 766 405 <sup>3)</sup>	10 828	12 930 <sup>+210</sup> <sub>-220</sub>	1.7	3.67	3.16 <sup>+0.08</sup> <sub>-0.08</sub>	0.08	0.0 <sup>+1.2</sup> <sub>-0.0</sub>	1.2	240 <sup>+12</sup> <sub>-12</sub>	5.0	B8	B9 IV	B7 III
10 960 750		19 960 <sup>+880</sup> <sub>-880</sub>	4.4		3.91 <sup>+0.11</sup> <sub>-0.11</sub>	0.11	0.0 <sup>+3.1</sup> <sub>-0.0</sub>	3.1	253 <sup>+15</sup> <sub>-15</sub>	5.9	B8	–	B2.5 V
11 973 705 <sup>4)</sup>	7 404	(11 150)		(4.04)	(3.96)		(3.9)		103 <sup>+10</sup> <sub>-10</sub>	9.7	B9	A9 V-IV	B8.5 V-IV
12 207 099 <sup>3)</sup>	10 711	(<11 000)		4.07	<3.1		(2.5)		43 <sup>+5</sup> <sub>-3</sub>	9.3	A0	B9 V	B9 III–II
12 258 330	13 224	14 700 <sup>+200</sup> <sub>-200</sub>	1.4	4.86	3.85 <sup>+0.04</sup> <sub>-0.04</sub>	0.04	0.0 <sup>+0.8</sup> <sub>-0.0</sub>	0.8	130 <sup>+8</sup> <sub>-8</sub>	6.2	B9 V	B7 V	B5.5 V-IV

<sup>1)</sup>binary, <sup>2)</sup>suspected SB2, RV var., <sup>3)</sup>suspected SB2, <sup>4)</sup>SB2

**Table 6.** Metallicity and elemental abundances relative to solar ones in dex and He abundance in fractions of the solar one. Stars are sorted by  $T_{\text{eff}}$ .

KIC	$T_{\text{eff}}$	$\epsilon$	He	C	N	O	Mg	Si	S	Ca	Fe
8 451 410	8 490	+0.10±0.10	–	–	–	+0.03	+0.11	+0.03	–0.05	–0.47	+0.34
8 583 770	9 690	+0.18±0.09	0.89	–	–	+0.18	+0.31	+0.13	–0.20	+0.23	+0.24
8 389 948	10 240	+0.10±0.12	1.24	–	–	+0.23	+0.26	+0.28	±0.00	±0.00	+0.14
5 130 305	10 670	–0.07±0.11	1.13	–	–	+0.03	–0.04	+0.03	–0.05	–0.37	+0.09
12 207 099 <sup>1)</sup>	<11 000	(>0.8)	1.40	–	–	±0.00	+0.56	–0.47	–0.10	–0.62	+0.49
7 599 132	11 090	+0.06±0.10	0.89	–	–	+0.23	+0.16	+0.13	±0.00	–0.07	+0.09
11 973 705 <sup>1)</sup>	11 150	(0.00±0.12)	0.77	–	–	+0.33	+0.21	–0.57	–0.40	+0.43	+0.04
5 217 845	11 790	–0.06±0.10	1.08	+0.15	±0.00	±0.00	+0.31	+0.03	+0.05	+0.38	–0.11
8 177 087	13 330	–0.11±0.11	<b>1.70</b>	+0.20	–0.10	+0.23	+0.06	–0.12	–0.15	–0.17	–0.11
8 766 405	12 930	– <b>0.41±0.12</b>	1.11	–	<b>+1.10</b>	<b>+1.11</b>	–0.09	– <b>0.37</b>	– <b>0.30</b>	–	– <b>0.56</b>
12 258 330	14 700	– <b>0.30±0.16</b>	<b>2.10</b>	±0.00	±0.00	–0.07	–0.14	–0.03	–0.30	–	–0.16
5 479 821	14 810	(–0.11±0.15)	<b>0.46</b>	<b>+0.95</b>	<b>+1.56</b>	±0.00	– <b>0.64</b>	+0.13	– <b>0.40</b>	–	+0.29
8 459 899	15 760	– <b>0.45±0.11</b>	1.47	+0.05	±0.00	<b>+0.38</b>	– <b>0.54</b>	– <b>0.47</b>	– <b>0.35</b>	–	– <b>0.46</b>
3 756 031	15 980	– <b>0.57±0.08</b>	1.49	–0.20	–0.09	<b>+0.38</b>	– <b>0.44</b>	– <b>0.67</b>	– <b>0.60</b>	–	– <b>0.36</b>
10 960 750	19 960	–0.04±0.16	1.00	±0.00	±0.00	±0.00	±0.00	±0.00	±0.00	–	±0.00
3 240 411	20 980	– <b>0.30±0.14</b>	1.40	– <b>0.30</b>	+0.06	–0.12	–0.19	– <b>0.92</b>	– <b>0.55</b>	–	– <b>0.46</b>
KIC	$T_{\text{eff}}$		Na	Sc	Ti	Cr	Mn	Y	Ba		
8 451 410	8 490		– <b>0.58</b>	– <b>2.01</b>	–0.11	+0.40	+0.25	<b>+0.93</b>	<b>+1.57</b>		
8 583 770	9 690		–	±0.00	+0.24	+0.30	<b>+0.50</b>	<b>+1.13</b>	–		
8 389 948	10 240		–	±0.00	–0.26	–0.20	–	–	–		
5 130 305	10 670		–	–	–0.01	–0.05	–	–	–		
12 207 099 <sup>1)</sup>	<11 000		–	–	–0.16	+2.30	±0.00	–	–		
7 599 132	11 090		–	–	+0.09	+0.10	–	–	–		

<sup>1)</sup>formal solution, suspected SB2 star

### 3.3. Results

Table 5 lists the fundamental parameters obtained for the 16 target stars.  $T_{\text{eff}}$  and  $\log g$  taken from the KIC are given for comparison. The  $1\sigma$ -errors of  $T_{\text{eff}}$  and  $v \sin i$  are given in per cent of the determined values, all other errors are absolute values. The spectral types are compared between those given in the SIMBAD

database at CDS, those derived from the  $T_{\text{eff}}$  and  $\log g$  listed in the KIC, and from our values of  $T_{\text{eff}}$  and  $\log g$ . For the derivation we used an interpolation based on the tables by Schmidt-Kaler (1982) and by de Jager & Nieuwenhuijzen (1987).

The accuracy in  $T_{\text{eff}}$  is about 2% (mean value of 1.8%) for most of the stars, only for the two hottest stars we obtain twice this value. Looking for any correlations between the errors of

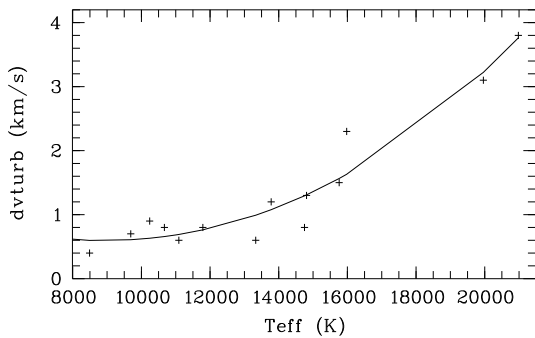


**Fig. 2.** Error in  $\xi_t$  versus measured  $T_{\text{eff}}$ .

measurement and the absolute values of determined parameters, we found only one, namely for the micro-turbulent velocity in dependence on  $T_{\text{eff}}$  (Fig. 2). It seems that our method can determine  $\xi_t$  with an accuracy of about  $0.6 \text{ km s}^{-1}$  for the cooler stars but that the error raises up to almost  $4 \text{ km s}^{-1}$  for the hottest stars. It means that for stars hotter than about  $15\,000 \text{ K}$  it is not possible to determine their micro-turbulent velocity and that for those stars the determination of the other parameters is practically independent of the value of  $\xi_t$ . There is also a slight correlation between the relative error of  $\nu \sin i$  and  $\log g$  that we attribute to the fact that the accuracy of  $\nu \sin i$  is lowered by the inclusion of  $H_\beta$  into the measurement and that for lower  $\log g$  the Balmer lines show narrower profiles. Due to the inclusion of  $H_\beta$ , the mean accuracy of our  $\nu \sin i$  determination is of only 8%. The mean error in  $\log g$  is of 0.07. We refer to the previous section where it was shown that all the errors get larger (and more reliable) by determining them from the complete grid in all parameters as we did here.

Table 6 lists the resulting metallicities and individual abundances. The upper part gives the abundances of elements that were found in the spectra of most of the stars, the lower part those that have been additionally found for the cooler stars. Larger deviations from the solar values are highlighted in bold face. The solar values refer to the solar chemical composition given by Grevesse et al. (2007). In the following, we give remarks on peculiarities found in some of the stars. A general comparison of our results with the KIC data will be given in Sect. 6.2.

*KIC 3 240 411 and 10 960 750:* Not any data about these two stars from previous investigations could be found. According to our measurement, they are the hottest stars of our sample. KIC 3 240 411 has low metallicity, in agreement with a distinct depletion in Fe, whereas KIC 10 960 750 has solar abundance.

*KIC 3 756 031:* This star shows the lowest metallicity of our sample. All metals where we found contributions in its spectrum are depleted, whereas He is enhanced. The profiles of some of the metal lines are strongly asymmetric. This may indicate pulsation (we will show that the star falls into the SPB instability region) or, because of the chemical peculiarity of the star, rotational modulation due to spots (as found, e.g., by Briquet et al. (2004) for four B-type stars showing inhomogeneous surface abundance distributions).

*KIC 5 217 845:* The star has been identified from the Kepler satellite light curve as eclipsing binary of uncertain type with a period of 1.67838 days (Prsa et al. 2010). No RV or line profile variations could be detected from our two spectra, however.

*KIC 5 479 821:* The star is He-weak by a factor of 0.46 compared to the solar value. It shows a strong enhancement of C and N and a depletion of Mg and S. All final parameter values

have been calculated from atmosphere models based on the derived individual abundances. The given metallicity, derived from a previous step, has no physical meaning.

*KIC 8 177 087:* This is the sharpest-lined star of our sample with  $\nu \sin i = 22 \text{ km s}^{-1}$ . Whereas He is strongly enhanced, all metal abundances are close to the solar values.

*KIC 8 451 410:* This is a suspected SB2 star. We observe a RV shift between our two spectra and cannot fit the shifted and co-added spectrum as perfect as in the other cases. The observed strong Ba and Y overabundance and the strong depletion in Sc may be related to the presence of a second component in the observed spectrum. The determined low temperature of about  $8\,500 \text{ K}$  agrees within the errors of measurement with that given in the KIC.

*KIC 8 459 899:* We suspect, from the slightly larger O-C residuals of the spectrum fit, that this star may be a SB2 star as well but that the obtained parameters are still reliable. It has low metallicity, the derived value agrees well with the depleted metal abundances, except for O which is enhanced.

*KIC 8 583 770:* This is a double star (WDS 19570+4441) with a 3-magnitude fainter companion at a separation of  $0.9''$ . According to our analysis, it is Si-strong, also Mg is enhanced.

*KIC 8 766 405:* The star has low metallicity, the derived value agrees well with the depleted metal abundances, except for N and O which are enhanced.

*KIC 11 973 705:* This is certainly a SB2 star, the typical spectrum of a cooler star of  $8\,000$  to  $9\,000 \text{ K}$  can be seen in the O-C residuals. All values given here result from a formal solution for the hotter component that shows the stronger lines. Due to the unknown flux ratio between the two components, the derived values, except for  $\nu \sin i$ , are not reliable.

*KIC 12 207 099:* For this sharp-lined star we have got no satisfactory solution. Maybe that it is a Chromium star (we obtain a Cr abundance of 2.30 dex above the solar one) and vertical stratification of the elemental abundances has to be included into the calculations, or it is a SB2 star as well.

*KIC 12 258 330:* The star is He-strong, it shows an enhancement in He abundance by a factor of more than two compared to the solar value. The metal abundances are close to the solar values, the derived metallicity is too low (see the remark for KIC 5 479 821).

#### 4. NLTE based analysis

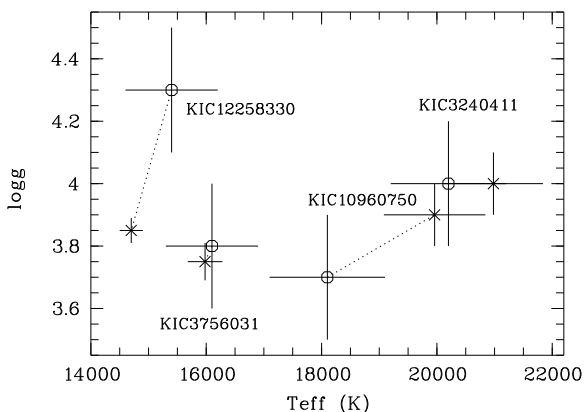
Our aim in this attempt was not to investigate the NLTE effects in detail but to check for the order of the deviations in the results of the LTE calculations that may arise from neglecting these effects. We used the GIRFIT program (Frémat et al. 2006) to determine the fundamental parameters  $T_{\text{eff}}$ ,  $\log g$ , and  $\nu \sin i$ . This program adjusts synthetic spectra interpolated on a grid of stellar fluxes to the observed spectra using the least squares method. The temperature structure of the atmospheres was computed as in Castelli & Kurucz (2003) using the ATLAS9 computer code (Kurucz 1993a). Non-LTE level populations were then computed for each of the atoms listed in Table 7 using the TLUSTY program (Hubeny & Lanz 1995) and keeping the temperature and the density distributions obtained with ATLAS9 fixed. For the spectral region considered, we used the specific intensity grids computed by Frémat (private communication) for  $T_{\text{eff}}$  and  $\log g$  ranging from  $15\,000 \text{ K}$  to  $27\,000 \text{ K}$  and from 3.0 to 4.5, respectively. For  $T_{\text{eff}} < 15\,000 \text{ K}$  we used LTE calculation. We assumed solar metallicity and a micro-turbulence of  $2 \text{ km s}^{-1}$  for all the grids.

**Table 7.** Atomic models used for the treatment of NLTE.

atom	ion	levels
Hydrogen	H I	8 levels + 1 superlevel
	H II	1 level
Helium	He I	24 levels
	He II	20 levels
	He III	1 level
Carbon	C II	53 levels, all individual levels
	C III	12 levels
	C IV	9 levels + 4 superlevels
	C V	1 level
Nitrogen	N I	13 levels
	N II	35 levels + 14 superlevels
	N III	11 levels
	N IV	1 level
Oxygen	O I	14 levels + 8 superlevels
	O II	36 levels + 12 superlevels
	O III	9 levels
	O IV	1 level
Magnesium	Mg II	21 levels + 4 superlevels
	Mg III	1 level

**Table 8.** Fundamental parameters derived from the NLTE model. LTE based values taken from Table 5 are given in parentheses.

Kepler-ID	$T_{\text{eff}}$ (K)	$\log g$	$v \sin i$ (km s $^{-1}$ )
KIC 3 240 411	20 200 $\pm$ 1000	4.0 $\pm$ 0.2	45 $\pm$ 15
	(20 980 $\pm$ 860)	(4.0 $\pm$ 0.1)	(43 $\pm$ 5)
KIC 10 960 750	18 100 $\pm$ 1000	3.7 $\pm$ 0.2	250 $\pm$ 20
	(19 960 $\pm$ 880)	(3.9 $\pm$ 0.1)	(253 $\pm$ 15)
KIC 3 756 031	16 100 $\pm$ 800	3.8 $\pm$ 0.2	40 $\pm$ 15
	(15 980 $\pm$ 300)	(3.75 $\pm$ 0.06)	(31 $\pm$ 4)
KIC 12 258 330	15 400 $\pm$ 800	4.3 $\pm$ 0.2	125 $\pm$ 15
KIC 12 258 330*	14 700 $\pm$ 800	4.1 $\pm$ 0.2	125 $\pm$ 15
	(14 700 $\pm$ 200)	(3.85 $\pm$ 0.04)	(130 $\pm$ 8)

\* based on  $H_{\beta}$  only**Fig. 3.** Comparison of the parameter values derived from LTE (crosses) and from NLTE (circles) treatment.

Our investigation of NLTE effects in the four hottest stars of our sample (not regarding the suspected SB2 candidates) is based on the 4720–5050 Å spectral region. For the hotter stars, we used the two helium lines at 4921 and 5016 Å that are present in this region to measure  $v \sin i$ . Then we determined the other parameters,  $T_{\text{eff}}$  and  $\log g$ , by fitting the spectrum in the whole domain between 4720 and 5050 Å. For the cooler stars of the sample, the determination of  $v \sin i$  is based on the metallic and the He I lines. The derived  $v \sin i$  values of these stars are con-

sistent with those obtained for the  $H_{\beta}$  lines. The coolest star, KIC 12 258 330, was analysed using LTE calculations to check for the influence of the usage of different wavelength ranges and the differences in the applied programs.

Table 8 lists the results. The given errors are computed according to the error determination method introduced by Martayan et al. (2006) that is based on the computation of theoretical spectra where a Poisson distributed noise has been added. For KIC 12 258 330, we did not find a satisfying solution that fits both the Balmer and the He lines and give two solutions here. For comparison, we also list the parameter values obtained in Sect. 3 and visualize the differences in the results in Fig. 3.

For two of the stars, among them the hottest star KIC 3 240 411, the values of both  $T_{\text{eff}}$  and  $\log g$  agree within the errors of measurement. For the other two stars, surprisingly for KIC 12 258 330 where we assumed LTE, we observe large differences between the values obtained from the two approaches. These results will be discussed in detail in Sect. 6.1.

## 5. Stellar temperatures from spectral energy distributions

### 5.1. The method

Stellar effective temperatures can be determined from the spectral energy distributions (SEDs). For our target stars, these were constructed from photometry taken from the literature. 2MASS (Skrutskie et al. 2006), Tycho B and V magnitudes (Høg et al. 1997), USNO-B1 R magnitudes (Monet et al. 2003), and TASS I magnitudes (Droege et al. 2006), supplemented with CMC14  $r'$  magnitudes (Evans et al. 2002) and TD-1 ultraviolet flux measurements (Carnochan 1979) where available.

The SED can be significantly affected by interstellar reddening. We have determined the reddening from interstellar NaD lines present in our spectra. For resolved multi-component interstellar NaD lines, the equivalent widths of the individual components were measured using multi-Gaussian fits. The total  $E(B-V)$  in these cases is the sum of the reddening per component, since interstellar reddening is additive (Munari & Zwitter 1997).  $E(B-V)$  was determined using the relation given by these authors. Several of stars have  $UBV$  photometry which allows us to determine  $E(B-V)$  using the Q-method (Heintze 1973). For these stars, there is good agreement with the extinction obtained from the NaD lines. The SEDs were de-reddened using the analytical extinction fits of Seaton (1979) for the ultraviolet and Howarth (1983) for the optical and infrared.

The stellar  $T_{\text{eff}}$  values were determined by fitting solar-composition (Kurucz 1993a) model fluxes to the de-reddened SEDs. The model fluxes were convolved with photometric filter response functions. A weighted Levenberg-Marquardt, non-linear least-squares fitting procedure was used to find the solution that minimizes the difference between the observed and model fluxes. Since  $\log g$  is poorly constrained by our SEDs, we fixed  $\log g=4.0$  for all the fits.

### 5.2. Results

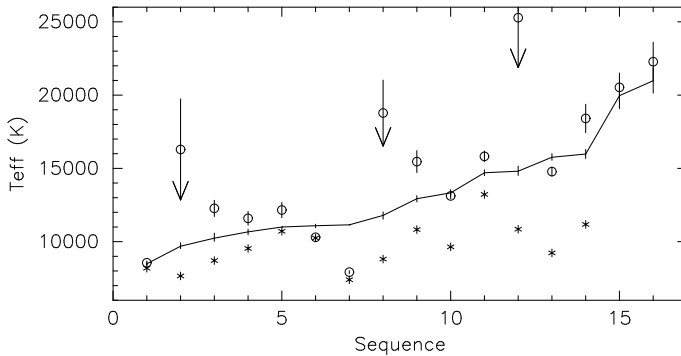
The results are given in Table 9. The uncertainty in  $T_{\text{eff}}$  includes the formal least-squares error and that from the uncertainty in  $E(B-V)$  added in quadrature. The differences between the photometric, spectroscopic, and the KIC values are shown in Fig. 4.

KIC 10 960 750 has  $uvby\beta$  photometry. Using the  $uvby\beta$  and  $TEFFLOGG$  codes of Moon (1985), we obtain  $E(B-V)=0.05$ ,

**Table 9.**  $E(B-V)$  determined from the Na D lines and from the Q-method, and  $T_{\text{eff}}$  obtained from SED-fitting.

KIC	$E(B-V)$	$T_{\text{eff}}$		SED Notes
		Na D	QM	
3 240 411	0.07±0.01		22 280±1 320	CMC14 $r'$
3 756 031	0.12±0.01*		18 470± 970	CMC14 $r'$
5 130 305	0.09±0.01		11 590± 470	CMC14 $r'$
5 217 845	0.25±0.03		18 780±2 250	CMC14 $r'$
5 479 821	0.24±0.03		25 280±3 390	
7 599 132	0.02±0.01		10 300± 130	CMC14 $r'$ , TD1
8 177 087	0.12±0.01	0.09	13 120± 200	TD1
8 389 948	0.20±0.02	0.19	12 270± 550	CMC14 $r'$ , TD1
8 451 410	0.04±0.01		8 560± 120	CMC14 $r'$
8 459 899	0.13±0.01*	0.16	14 780± 310	TD1
8 583 770	0.38±0.06		16 290±3 440	CMC14 $r'$
8 766 405	0.10±0.01*	0.12	15 460± 750	
10 960 750	0.06±0.01	0.06	20 530± 980	CMC14 $r'$ , TD1
11 973 705	0.02±0.01*		7 920± 100	TD1
12 207 099	0.03±0.01		12 160± 520	
12 258 330	0.04±0.01	0.08	15 820± 370	TD1

\* indicates multi-component interstellar Na D lines

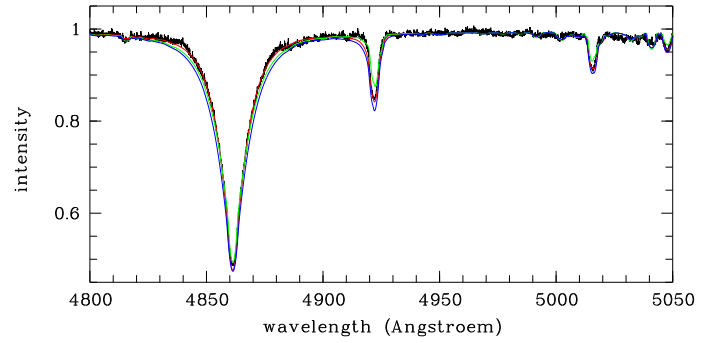
**Fig. 4.** Comparison of  $T_{\text{eff}}$  given in the KIC (asterisks) with the spectroscopic (connected by lines) and photometric (open circles) values. The stars are sorted by their spectroscopically determined temperature.

$T_{\text{eff}}=19320\pm800$  K, and  $\log g=3.60\pm0.07$ , which is in good agreement with what we determined from spectroscopy. For three more stars, the  $T_{\text{eff}}$  derived from SED fitting agree with those from the spectroscopic analysis within the errors of measurement. For 12 of the 16 targets, the photometric  $T_{\text{eff}}$  is close to the spectroscopic  $T_{\text{eff}}$  confirming the spectroscopically obtained values. In only one case, for KIC 11 973 705, the photometric  $T_{\text{eff}}$  is in favour of the KIC value. This is the star that we identified as a SB2 star where we see the lines of a secondary component in its spectrum. KIC 5 217 845, 5 479 821 and 8 583 770 suggest that the interstellar lines comprise of unresolved multiple components leading to an overestimation of the interstellar reddening and to much too high  $T_{\text{eff}}$ . One of them, KIC 8 583 770, is a double star (WDS 19570+4441) with a 3-magnitude fainter companion at a separation of 0.9".

## 6. Discussion

### 6.1. The influence of NLTE effects

Four stars have been analysed by two different methods using a) slightly different input physics, b) LTE or NLTE treatment for three of the stars, and c) different wavelength ranges, short in NLTE, wider in LTE. For two of the stars, KIC 3 240 411

**Fig. 5.** Fit of the spectrum of KIC 12 258 330 obtained from models 1 (red), 2 (green), and 3 (blue).

and KIC 3 766 081, the results agree well within the errors of measurement. For the other two stars, KIC 10 960 750 and KIC 12 258 330, we find significant deviations. The fact that we find a good agreement for the hottest star and a distinct deviation for the coolest one that was analysed using LTE in both attempts, is surprising and raises questions about the origin of the observed deviations, i.e. about the order of the influence of the differences in the two methods that we labeled a) to c) in before.

For KIC 12 258 330, we can clearly show that the difference in the results comes from the facts that it is a helium-strong star and that our second approach assumed solar metallicity and He abundance. Fig. 5 shows the quality of different fits, all calculated in LTE. Model 1 is the original LTE solution with the He abundance enhanced by a factor of 2.1 against the solar one and  $T_{\text{eff}}=14700$  K,  $\log g=3.85$ . Models 2 and 3 are based on  $T_{\text{eff}}=15400$  K,  $\log g=4.30$  with solar He abundance in model 2 and enhanced He abundance in model 3. It can be seen that varying the He abundance effects not only the strength of the He lines but also the shape of the wings of  $H_{\beta}$  and so the derived  $\log g$ . Compared to solution 1), the reduced  $\chi^2$  of solution 2) is 1.5 times higher and that of solution 3) 3.2 times higher. We assume that the parameter values derived in Sect. 3 are the correct ones and that KIC 12 258 330 is helium-strong.

A closer investigation of the application to KIC 10 960 750 shows that the differences in  $T_{\text{eff}}$  and  $\log g$  mainly come from the usage of different wavelength regions. If we shorten the region for the LTE calculations to that used in NLTE we end up with  $T_{\text{eff}}=(18940\pm840)$  K and  $\log g=3.78\pm0.08$  which comes much closer to the results obtained from the NLTE calculations. Here, we have to solve the question if the difference in the results comes from the fact that one more stronger He line at 5876 Å was included in the wider spectral range used in the LTE approximation which falsifies the LTE results due to additional NLTE effects, or if the difference simply comes from the fact that a wider spectral range gives more accurate results which favours the LTE results.

As already mentioned in the introduction, Auer & Mihalas (1973) state that the deviations in the equivalent widths of the He lines due to the effects of departure from NLTE increases for B-type stars with wavelength and can reach 30% for the 5 876 Å line and more for redder lines. According to their calculations, NLTE effects are negligible only for the He lines in the blue (up to He I 4471 Å) but produce deeper line cores for the He lines at longer wavelengths whereas the line wings remain essentially unaffected. Hubeny & Lanz (2007) state as well that the core of strong lines and lines from minor ions will be most affected by departures from LTE which implies that the abundance of some species might be overestimated from LTE predictions. Also the

surface gravities derived from the Balmer line wings tend to be overestimated.

Mitskevich & Tsymbal (1992), on the other hand, computed model atmospheres of B-stars in LTE and NLTE and found no remarkable differences. In particular the temperature inversion in the upper layers of the atmospheres, intrinsic to the models of Auer & Mihalas, is absent in their NLTE models and the departure coefficients for the first levels of H and He in the upper layers are lower by three orders of magnitude. The authors believe that the reason for the discrepancy in the results is the absence of agreement between radiation field and population levels in the program applied by Auer & Mihalas. And there is a second point. The TLUSTY program (Hubeny & Lanz 1995) provides NLTE fully line-blanketed model atmospheres, whereas Auer & Mihalas did not take the line blanketing into account.

In a more recent article, Nieva & Przybilla (2007) investigate the NLTE effects in OB stars. Using ATLAS 9 for computing the stellar atmospheres in LTE and the DETAIL and SURFACE programs to include the NLTE level populations and to calculate the synthetic spectra, respectively, they compute the Balmer and He I, II lines over a wide spectral range and compare the results with those of pure LTE calculations. In the result, they obtained narrower profiles of the Balmer lines in LTE compared to NLTE for stars hotter than 30 000 K, leading to an overestimation of their surface gravities. The calculations done for one cooler star of 20 000 K which is in the range of the hottest stars of our sample, but for  $\log g$  of 3.0, did not show such effect but differences in the line cores, increasing from  $H_\delta$  to  $H_\alpha$ . The same they observed for the cooler star for the He I lines. Many of them experience significant NLTE-strengthening, in particular in the red, but without following a strong rule. So the strengthening of the He I 5876 Å line is less than that of the 4922 Å and 6678 Å lines.

From the LTE calculations, we obtain solar metal and He abundance for KIC 10 960 750. Unfortunately, our actually available grid of NLTE synthetic spectra does not comprise the wavelength region of the He I 5876 Å line and so we cannot reproduce the LTE calculations one by one. Since the quality of the fit of the observed spectrum obtained from the LTE and NLTE calculations is the same we can not directly decide if the difference in the parameters comes from NLTE effects of the He 5876 Å line as discussed above. But since we do not observe any deviation in the results for the hottest star of our sample, we believe that NLTE effects are only second order effects and cannot give rise to the deviations observed for KIC 10 960 750.

## 6.2. Comparison with the KIC data

Comparing our  $T_{\text{eff}}$  and  $\log g$  with the values given for 12 of the stars in the KIC (for two of the 16 stars of our sample there are no entries, and we excluded KIC 11 973 705 and 12 207 099), we see systematic differences. We obtain higher temperatures in general, the difference increases with increasing temperature of the stars. Already Molenda-Żakowicz et al. (2010) found that the  $T_{\text{eff}}$  given in the KIC is too low for stars hotter than about 7 000 K, by up to 4 000 K for the hottest stars. The trend in the temperature difference derived from our values is shown in Fig. 6 (the error in the difference also includes the 200 K error typical for the KIC data). We have drawn the curve of a second order polynomial resulting from a fit that observes the boundary condition that the difference should be zero for  $T_{\text{eff}}=7 000$  K. Our analysis seems to confirm the finding by Molenda-Żakowicz et al.

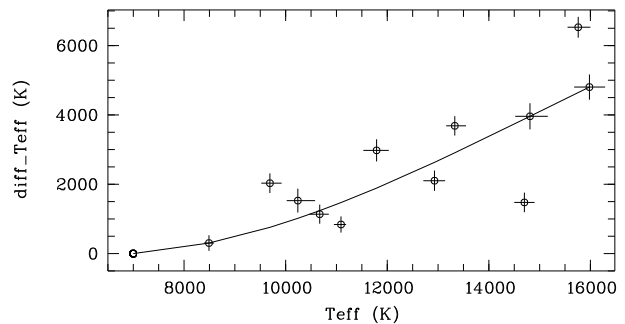


**Fig. 6.** Difference in  $T_{\text{eff}}$  between our values and those given in the KIC versus measured  $T_{\text{eff}}$ .

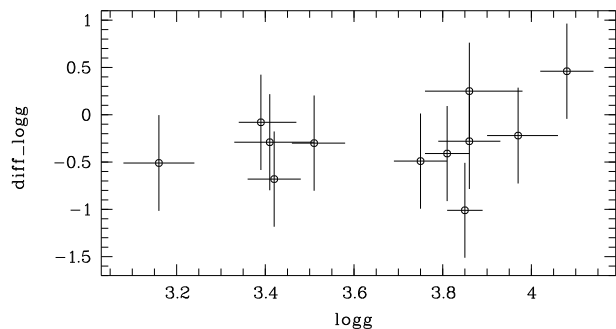


**Fig. 7.** Difference in  $\log g$  between our values and those given in the KIC versus measured  $\log g$ .

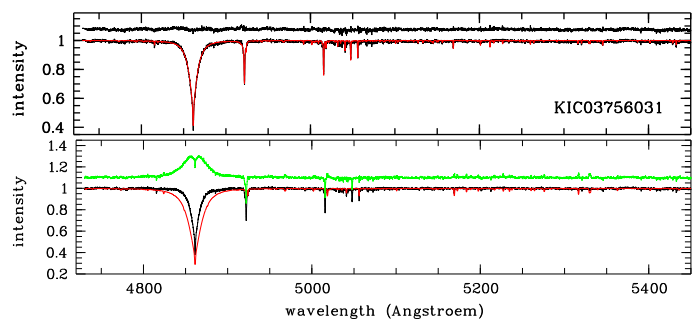


**Fig. 8.** Fit (red) of the spectrum of K03758031 (black), assuming  $T_{\text{eff}}=16 000$  K (top) and  $T_{\text{eff}}=11 200$  K (bottom). The O–C spectra are shifted by +1.1.

Comparing our values derived for  $\log g$  with those given in the KIC, we find that they are systematically lower (Fig. 7). Counting for the large errors that mainly result from the  $\pm 0.5$  dex error of the KIC data, we cannot say that this difference is sig-

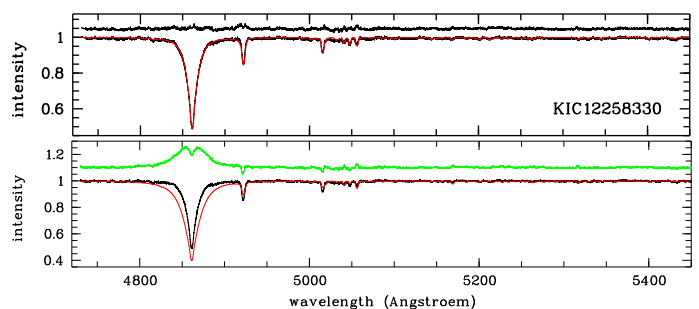


**Fig. 9.** As Fig. 8 but for KIC 12 258 330 and  $T_{\text{eff}}=14 750$  K,  $\log g=3.85$  (top) and  $T_{\text{eff}}=13 224$  K,  $\log g=4.86$  (bottom).

nificant, however. The same holds true for the Fe/H ratios given in the KIC, the corresponding error of  $\pm 0.5$  dex prevents us from any comparison with our derived values.

There are two extreme cases: KIC 3 756 031, where our derived temperature is 16 000 K whereas the KIC gives about 11 200 K, and KIC 12 258 330, where we obtain a  $\log g$  of 3.85 which is by 1 dex lower than given in the KIC. A closer investigation shows, however, that the KIC values are very unlikely.

Fig. 8 shows, in its upper panel, the fit of a part of the spectrum of KIC 3 756 031 assuming our value of  $T_{\text{eff}}$ . The lower panel gives the same for  $T_{\text{eff}}$  taken from the KIC. Neither  $H_{\beta}$  nor the He lines are fitted well. The best fit of  $H_{\beta}$  at this temperature is obtained assuming a  $\log g$  below 3.0, but in this case the He lines can also not be reproduced. The use of LTE in our program cannot balance a temperature difference of 5 000 K and the 11 200 K given in the KIC cannot be true for this star.

Fig. 9 shows, in its upper panel, the fit of a part of the spectrum of KIC 12 258 330 assuming our values of  $T_{\text{eff}}$  and  $\log g$ . The lower panel gives the same for  $T_{\text{eff}}$  and  $\log g$  taken from the KIC. The resulting deviation in the shape of  $H_{\beta}$  cannot be explained in terms of a wrong continuum normalization in the  $H_{\beta}$  range. The  $\log g$  given for this star in the KIC is by about 1 dex too large.

### 6.3. $T_{\text{eff}}$ from spectral energy distributions

Our method of deriving  $E(B-V)$  from the EWs of the Na D lines may overestimate  $T_{\text{eff}}$  in the cases where we observe non-resolved interstellar contributions to the Na D line profiles. This is one reason, besides the poor photometric data for some of the stars, why this method is of lower accuracy compared to the spectroscopic analysis. The facts that the  $E(B-V)$  derived from the Na D lines and from the Q-method for the stars where  $UBV$  or, in one case,  $uvby\beta$  photometry was available are in a good agreement and that all derived  $T_{\text{eff}}$  are in favour of our spectroscopic values confirm that the  $T_{\text{eff}}$  given in the KIC must be too low, however.

Thus, the results from the SED-fitting based on the photometric data reveal the reason why the  $T_{\text{eff}}$  given in the KIC deviate from our findings. For most of the hotter stars, the interstellar reddening was not properly taken into account leading to an underestimation of the stellar temperatures. It also explains why the difference in the derived temperatures between the KIC and our spectroscopic analysis rises with increasing temperature of the stars. The hotter the stars, the more luminous and the farther they are and the more the ignored reddening plays a role.

### 6.4. Positions of the stars compared to SPB and $\beta$ Cep instability strips

In the result of our analysis, we can directly place the stars into a  $T_{\text{eff}}-\log g$  diagram to compare their positions with the known instability domains of main-sequence B-type pulsators. Fig. 10 shows the resulting plots where the boundaries of the theoretical  $\beta$ Cep (the hottest region in Fig. 10) and SPB instability strips have been taken from Miglio et al. (2007). A core convective overshooting parameter of 0.2 pressure scale heights was used in the stellar models since asteroseismic modeling results of  $\beta$ Cep targets have given evidence for the occurrence of core overshooting of that order (e.g. Aerts et al. 2010). It is well-known that the choice of the metal mixture, opacities and metallicity also has a large influence on the extent of the instability regions. Here, we illustrate these domains for the OP (upper panel) and the

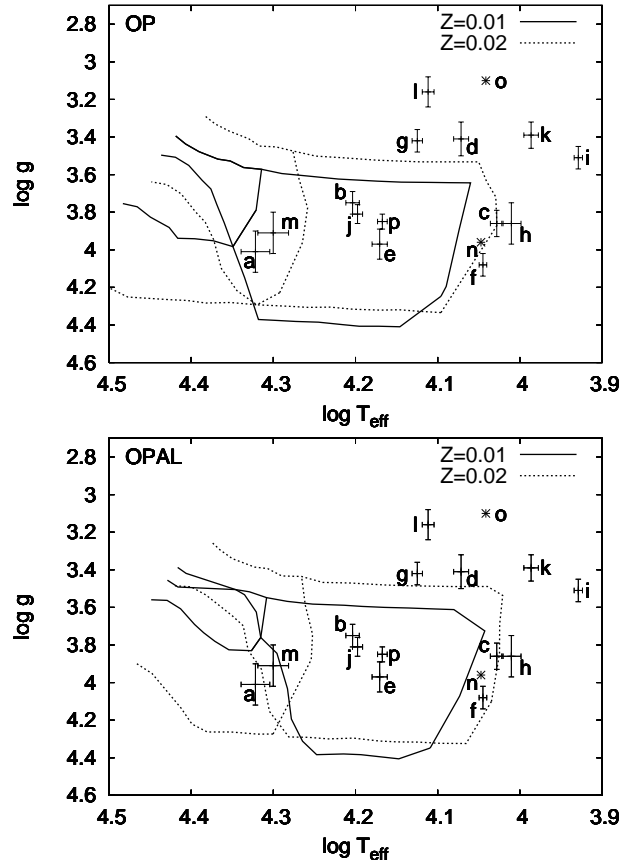


**Fig. 10.** Positions of the stars and the SPB and  $\beta$ Cep instability regions in the  $T_{\text{eff}}-\log g$  diagram.

**Table 10.** Positions of the stars with respect to the instability regions.

position	KIC	spectral type	$N$
$\beta$ Cep/SPB	3 240 411	B2 V	a
	10 960 750	B2.5 V	m
SPB	3 756 031	B5 IV-V	b
	5 479 821	B5.5 V	e
	8 459 899	B4.5 IV	j
	12 258 330	B5.5 IV-V	p
possibly SPB	5 130 305	B9 IV-V	c
	5 217 845	B8.5 III	d
	7 599 132	B8.5 V	f
	8 177 087	B7 III	g
	8 389 948	B9.5 IV-V	h
too cool	8 451 410	A3.5 IV-III	i
	8 583 770	A0.5 IV-III	k
too evolved	8 766 405	B7 III	l
uncertain	11 973 705	B8.5 VI-V	n
(SB2 stars)	12 207 099	B9 II-III	o

OPAL (lower panel) opacity tables, as well as for two values of the metal mass fraction  $Z=0.01$  (continuous boundaries of the instability regions) and  $Z=0.02$  (dashed boundaries). However, we only adopt the metal mixture by Asplund et al. (2005) corrected with the Ne abundance determined by Cunha et al. (2006). Another choice of metal mixture (e.g., that by Grevesse & Noels 1993) leads to narrower instability domains, as shown in Miglio et al. (2007).

The stars in Fig. 10 are marked by the letters given in Table 10. The SB2 star KIC 11 973 705 and the other presumed SB2 star KIC 12 207 099 are marked by two asterisks, as their determined values are uncertain and no error bars can be given. It can be seen that 4 stars (b, e, j and p) fall into the middle of the SPB region. The two hottest stars (a and m) can be of SPB and/or  $\beta$ Cep nature. Both low order p- and g-modes, and high-order g-modes can be expected for these possibly 'hybrid' pulsators. Six of the stars (c, d, f, g, h and n) lie on or close to the boundaries of the SPB instability strips so that they possibly exhibit high-order g-mode pulsations. The remaining 4 stars lie outside the instability regions, two of them (k and i) are too cool to be main-sequence SPB stars and the two other ones (l and o) have too low  $\log g$ . Table 10 lists the potential pulsators together with their spectral types as derived in Sect. 3.3. For the two suspected SB2 stars we do not want to make a classification in terms of pulsators because their determined spectral types may be completely wrong.

## 7. Conclusions

We tried to determine the fundamental parameters of B-type stars from the combined analysis of  $H\beta$  and the neighbouring metal lines in high-resolution spectra. Our results obtained for the test star Vega show that we can reproduce the values of  $T_{\text{eff}}$ ,  $\log g$ ,  $v \sin i$ , metallicity and micro-turbulent velocity known from the literature and that our method works well at least in the 10 000 K range.

The application of our programs to stars hotter than 15 000 K sets limitations in the accuracy of the results due to the used LTE approximation. The independent analysis of the four hottest stars of our sample by NLTE-based programs showed that the derived parameters agree within the errors of measurements for two of the stars, among them the hottest star. The deviations obtained for the other two stars can be explained by other limitations of the applied methods than the use of LTE and thus we believe that our results are valid within the derived errors of measurement.

In particular, the use of LTE cannot explain the large deviations in  $T_{\text{eff}}$  and  $\log g$  following for some of the stars from the KIC data, however, as we showed on two examples. From our results, there is strong evidence that the KIC systematically underestimates the temperatures of hotter stars, the difference increases with increasing  $T_{\text{eff}}$ . This finding confirms the results by Molenda-Żakowicz et al. (2010) which observed the same tendency for stars hotter than about 7 000 K.

The calculation of  $T_{\text{eff}}$  using SED-fitting based on the available photometric data revealed the reason why the  $T_{\text{eff}}$  listed in the KIC are too low and why the difference is largest for the hottest stars: the stellar temperatures have been underestimated because the interstellar reddening was not properly taken into account.

Eight stars of our sample show larger abundance anomalies. Five of them have reduced metallicity, two are He-strong, one is He-weak, and one is Si-strong.

According to our measurements, two of the 16 investigated stars fall into the overlapping range of the  $\beta$ Cep and SPB instability regions and could show, as so-called hybrid pulsators, both low-order p- and g-modes and high-order g modes. These are the two hottest stars in our sample, KIC 3 240 411 and KIC 10 960 750. Four stars fall into the SPB instability region, and five more are located close to the borders of this region. The two coolest stars, KIC 8 451 410, and KIC 8 583 770, lie between the SPB instability region and the blue edge of the classical instability strip. Two of the stars, KIC 11 973 705 and

KIC 12 207 099, could not be classified because of their SB2 nature and one star, KIC 8 766 405, is too evolved to show  $\beta$ Cep or SPB-type pulsations.

*Acknowledgements.* This research has made use of the SIMBAD database, operated at CDS, Strasbourg, France, the Vienna Atomic Line Database (VALD), and of data products from the Two Micron All Sky Survey, which is a joint project of the University of Massachusetts and the Infrared Processing and Analysis Center/California Institute of Technology, funded by the National Aeronautics and Space Administration and the National Science Foundation. T.S. is deeply indebted to Dr. Yves Frémat for providing the NLTE specific intensity grids for this study. A.T. and D.S. acknowledge the support of their work by the Deutsche Forschungsgemeinschaft (DFG), grants LE 1102/2-1 and RE 1664/7-1, respectively.

## References

- Aerts, C., Christensen-Dalsgaard, J., Kurtz, D. W. 2010, *Asteroseismology*, Springer
- Asplund, M., Grevesse, N., Sauval, A. J., Allende Prieto, C., & Blomme, R. 2005, *A&A*, 431, 693
- Auer, L.H. & Mihalas, D. 1973, *ApJS* 25,433
- Briquet, M., Aerts, C., Lüftinger, T. 2004, *A&A* 413, 273
- Carnochan, D.J., 1979, *Bull. Inf. CDS*, 17, 78
- Castelli, F. & Kurucz, R.L. 1994, *A&A* 281, 817
- Castelli, F. & Kurucz, R.L. 2003, *IAU Symp.* 210, 20
- Cunha, K., Hubeny, I., & Lanz, T. 2006, *ApJ*, 647, L143
- de Jager, C. & Nieuwenhuijzen, H. 1987, *A&A* 177, 217
- Dreiling, L.A. & Bell, R.A. 1980, *ApJ* 241,736
- Droege, T.F., Richmond, M.W., Sallman, M., 2006, *PASP*, 118, 1666
- Evans, D.W., Irwin, M.J., Helmer, L., 2002, *A&A*, 395, 347
- Frémat, Y., Zorec, J., Hubert, A.-M., et al., 2005, *A&A*, 440, 305
- Frémat, Y., Neiner, C., Hubert, A.-M., et al. 2006, *A&A*, 451, 1053
- Gigas, D. 1986, *A&A* 165, 170
- Grevesse, N. & Noels, A. 1993, in *La formation des éléments chimiques*, AVCP, ed. R.D. Hauck B., Paltani S., p. 205
- Grevesse, N., Asplund, M., Sauval, A. J. 2007, *Space Sci. Rev.* 130, 105
- Heintze, J.R.W. 1973, *Proc. IAU Symp.* 54, p. 231.
- Hill, G., Gulliver, A.F., Adelman, S.J. 2004, *IAU Symp.* 224,35
- Høg, E., Bässgen, G., Bastian, U., et al. 1997, *A&A*, 323, 57
- Howarth, I.D., 1983, *MNRAS*, 203, 301
- Hubeny, I. & Lanz, T. 1995, *ApJ* 1995, 439, 875
- Hubeny, I. & Lanz, T. 2007, *ApJS* 169, 83
- Kupka, F., Ryabchikova, T.A., Piskunov, N.E., et al. 2000, *Baltic Astronomy* 9, 590
- Kurucz, R.L. 1979, *ApJS* 40, 1
- Kurucz, R.L. 1993a, *ATLAS9 Stellar Atmosphere Programs and 2 km/s grid*, Kurucz CD-ROM No. 13, Smithsonian Astroph. Obs.
- Kurucz, R.L. 1993b, *IAU Colloquium* 138, 87
- Lane, M.C. & Lester, J.B. 1984, *ApJ* 281, 723
- Martayan, C., Frémat, Y., Hubert, A.-M., et al., 2006, *A&A*, 452, 273
- Miglio, A., Montalbán, J., Dupret, M.-A. 2007, *CoAst*, 151, 48
- Mitskevich, A.S., Tsymbal, V.V. 1992, *A&A* 260, 303
- Molenda-Żakowicz, J., Jerzykiewicz, M., Frasca, A., et al. 2010, submitted (arXiv:1005.0985)
- Monet, D.G., Levine, S.E., Casian, B., et al. 2003, *AJ*, 125, 984
- Moon, T.T., 1985, *Commun. Univ. London Obs.*, 78
- Munari, U., Zwitter, T., 1997, *A&A*, 318, 26
- Nieva, M.F. & Przybilla, N. 2007, *A&A*, 467, 295
- Prsa, A., Batalha, N.M., Slawson, R.W., 2010, *AJ*, submitted (arXiv:1006.2815)
- Schmidt-Kaler, Th. 1982, in Schaifers, K. & Voigt, H.H. (eds.) *Landolt-Börnstein Vol. 2b*, Springer-Verlag 1982
- Seaton, M.J., 1979, *MNRAS*, 187, 73
- Shulyak, D., Tsymbal, V., Ryabchikova, et al. 2004, *A&A* 428, 993
- Skrutskie, M.F., Cutri, R.M., Stiening, R., et al., 2006, *AJ*, 131, 1163
- Tsymbal, V. 1996, *ASPC* 108, 198